An Effective Reluctivity Model for Nonlinear and Anisotropic Materials in Time-Harmonic Finite Element Computations

Hans Vande Sande[1], François Henrotte[2], Herbert De Gersem[3], and Kay Hameyer[2]

[1]Atlas Copco Airpower n.v., Airtec Division, Boomsesteenweg 957, B-2610, Wilrijk, Belgium
[2]Rheinisch-Westfälische Technische Hochschule, Institut für Elektrische Maschinen, D-52056 Aachen, Germany
[3]Technische Universität Darmstadt, Institut für Theorie Elektromagnetischer Felder, D-64289 Darmstadt, Germany

In time-harmonic finite element analysis, the nonlinear behavior of soft-magnetic materials is often modeled by effective reluctivity curves, to account for the time-dependence of the reluctivity during one cycle of the applied sinusoidal signal. In this paper, the effective reluctivity concept is generalized in such a way, that nonlinear and anisotropic materials can be modeled as well. The model is used to simulate the flux line distribution and the loss distribution in a three-phase transformer under no-load operation.

***Index Terms*—Anisotropic media, finite element methods, harmonic analysis, nonlinear magnetics.**

I. Introduction

THE governing equation of a magnetodynamic problem is

$$\nabla \times (\nu \nabla \times \vec{A}) + \sigma \frac{\partial \vec{A}}{\partial t} = \vec{J}_{\rm s} \tag{1}$$

where ν is the reluctivity tensor [m/H], $\vec{A}$ the magnetic vector potential [Tm] and $\vec{J}_{\rm s}$ the current density of the externally applied current sources $[{\rm A/m^2}]$ [1]. In a time-harmonic formulation, the magnetic vector potential and the current density are supposed to vary sinusoidally. This means

$$\vec{A}(x,y,z,t) = \Re\left\{\vec{\tilde{A}}(x,y,z)e^{j\omega t}\right\}, \tag{2}$$

$$\vec{J}_{\rm s}(x,y,z,t) = \Re\left\{\vec{\tilde{J}}_{\rm s}(x,y,z)e^{j\omega t}\right\} \tag{3}$$

where the variables $\vec{\tilde{A}}(x,y,z)$ and $\vec{\tilde{J}}_{\rm s}(x,y,z)$ are vectors with phasor-valued components, represented by complex numbers. Introducing (2) and (3) in the magnetodynamic equation (1) yields the governing equation of the time-harmonic problem

$$\nabla \times (\underline{\nu} \nabla \times \vec{\tilde{A}}) + j\sigma\omega\vec{\tilde{A}} = \vec{\tilde{J}}_{\rm s}. \tag{4}$$

Since the reluctivity tensor entries may be complex-valued[1] as well, the tensor is indicated by $\underline{\nu}$.

When considering two-dimensional (2-D) problems, the time-harmonic equation (4) transforms into

$$\nabla \cdot (\underline{\nu}' \nabla \tilde{A}) - j\sigma\omega\tilde{A} = -\tilde{J}_{\rm s} \tag{5}$$

where $\underline{\nu}'$ is defined by

$$\underline{\nu}' = \begin{pmatrix} \underline{\nu}_{yy} & -\underline{\nu}_{yx} \\ -\underline{\nu}_{xy} & \underline{\nu}_{xx} \end{pmatrix} \tag{6}$$

being a reordering of the reluctivity tensor

$$\underline{\nu} = \begin{pmatrix} \underline{\nu}_{xx} & \underline{\nu}_{xy} \\ \underline{\nu}_{yx} & \underline{\nu}_{yy} \end{pmatrix}. \tag{7}$$

The magnetic flux density then equals

$$\vec{\tilde{B}} = \frac{\partial \tilde{A}}{\partial y}\vec{e}_x - \frac{\partial \tilde{A}}{\partial x}\vec{e}_y. \tag{8}$$

II. System Equations

When applying the finite element method for numerically solving (4) or (5), one basically has to solve the following algebraic system of complex equations:

$$\tilde{\mathbf{r}} = (\underline{\mathbf{K}} + \underline{\mathbf{L}})\tilde{\mathbf{A}} - \tilde{\mathbf{T}} = \mathbf{0} \tag{9}$$

where $\underline{\mathbf{K}}$, $\underline{\mathbf{L}}$, and $\tilde{\mathbf{T}}$ represent the diffusion term, the Helmholtz term and the source term, respectively. Vector $\tilde{\mathbf{r}}$ refers to the residual vector. The system (9) is nonlinear, due to the dependence of $\underline{\mathbf{K}}$ on $\underline{\nu}$. Since the entries of the reluctivity tensor may be complex-valued, the entries of the stiffness matrix may be complex-valued as well. By splitting $\underline{\mathbf{K}}$ into its real and imaginary part

$$\underline{\mathbf{K}} = \underline{\mathbf{K}}^{\rm re} + j\underline{\mathbf{K}}^{\rm im} \tag{10}$$

the system (9) transforms into

$$\tilde{\mathbf{r}}(\tilde{\mathbf{A}}) = \left[\underline{\mathbf{K}}^{\rm re}(\tilde{\mathbf{A}}) + j\left(\underline{\mathbf{L}}^{\rm im} + \underline{\mathbf{K}}^{\rm im}(\tilde{\mathbf{A}})\right)\right]\tilde{\mathbf{A}} - \tilde{\mathbf{T}} = \mathbf{0}. \tag{11}$$

It can be iteratively solved using the Newton–Raphson method [2], [3].

Digital Object Identifier 10.1109/TMAG.2005.845077

[1]The term *phasor-valued* and the corresponding notation with a tilde is reserved for complex-valued quantities that represent sinusoidally varying quantities. All other complex-valued quantities are underlined.

III. Effective Reluctivity Tensor Model

A. Phasor-Valued Flux Density

In time-harmonic simulations, the flux density is a vector with phasor-valued components, according to (8). The knowledge of $\vec{\tilde{B}}$ is required to evaluate the reluctivity tensor. Considering $\vec{\tilde{B}}$ in time-domain

$$\vec{B}(t) = \Re\{\vec{\tilde{B}} e^{j\omega t}\} \tag{12}$$

yields

$$B_x(t) = \tilde{B}_x^{\mathrm{re}} \cos\omega t - \tilde{B}_x^{\mathrm{im}} \sin\omega t \tag{13}$$
$$= |\tilde{B}_x| \cos(\omega t - \phi_x), \tag{14}$$
$$B_y(t) = \tilde{B}_y^{\mathrm{re}} \cos\omega t - \tilde{B}_y^{\mathrm{im}} \sin\omega t \tag{15}$$
$$= |\tilde{B}_y| \sin(\omega t - \phi_y). \tag{16}$$

Obviously, $\vec{B}$ generally describes an elliptic locus in in the $\{x, y\}$ plane. Hence, a phasor-valued vector potential solution allows for a variety of alternating and rotating fluxes in each finite element. This information has to be processed by a material model to obtain the time-harmonic reluctivity tensor entries.

B. Generalized Effective Reluctivity Concept

When applying an elliptically shaped $\vec{B}$-locus to a nonlinear and/or anisotropic material, it is observed that the measured $\vec{H}$-locus is generally not elliptic. In time-domain analysis, such behavior is modeled using a time-varying reluctivity tensor. Since this is impossible in time-harmonic analysis, one must approximate the relation between $\vec{B}$ and $\vec{H}$. The quality of the approximation is influenced by the following factors:

- *Nonlinearity*. If the materials are isotropic, an effective magnetization curve is usually extracted from the measured magnetization curve by an averaging rule based on integration [4]–[6]. Depending on the type of averaging, significant differences are observed in the saturation level of the effective magnetization curve.
- *Rotational fluxes*. These averaging techniques implicitly suppose that $\vec{B}$ or $\vec{H}$ are sinusoidally alternating along a line. This assumption is valid in the major part of an induction machine e.g., but it is not necessarily true in the region between teeth and yoke [7]. Since averaging the reluctivity is not required for circular fluxes, additional errors are introduced in the analysis if such an effective magnetization curve is used for rotational fluxes as well.
- *Anisotropy*. If an elliptical $\vec{B}$-locus is applied to a nonlinear and anisotropic material, it is observed that the shape of the $\vec{H}$-locus depends on the angle γ between the principal axes of the material and the $\vec{B}$ ellipse [8].

The idea behind effective magnetization curves can be generalized, taking into account these items. E.g.,

$$\underline{\nu} = \underline{\nu}\left(|\vec{B}|_{\max}, a, \gamma\right) \tag{17}$$

with

$$a = \frac{|\vec{B}|_{\min}}{|\vec{B}|_{\max}} \tag{18}$$

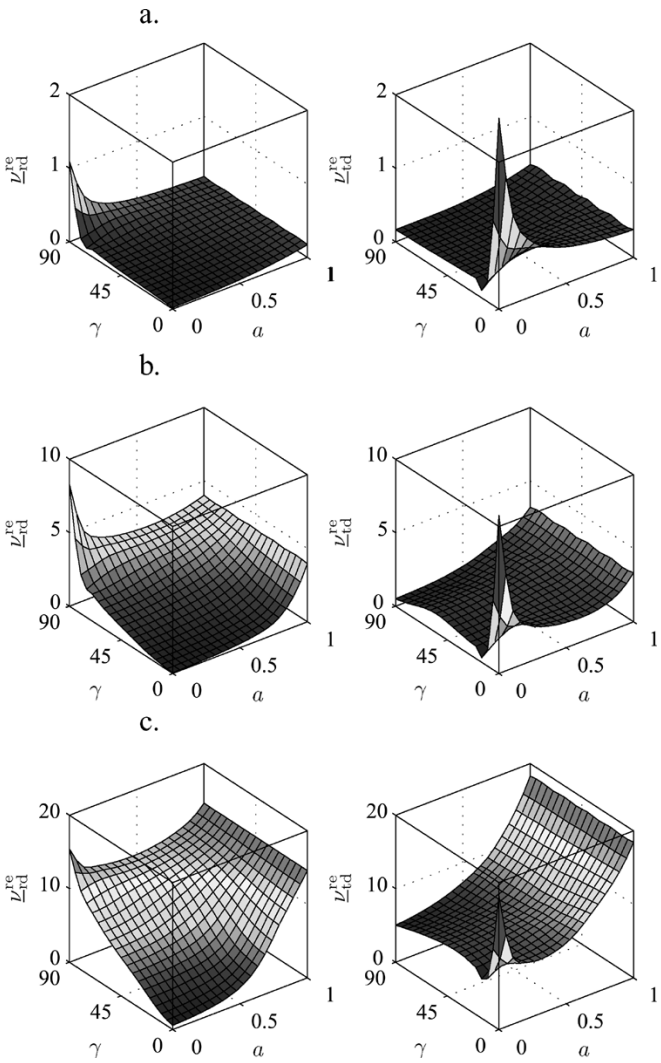

Fig. 1. Real part of the effective reluctivities $\underline{\nu}_{\mathrm{rd}}$ and $\underline{\nu}_{\mathrm{td}}$ [10^3 m/H] as a function of the aspect ratio a [$-$] and the inclination angle γ [°] of the $\vec{B}$-locus, for (a) $|\vec{B}|_{\max} = 0.55$ T, (b) $|\vec{B}|_{\max} = 1.38$ T and (c) $|\vec{B}|_{\max} = 1.93$ T. The imaginary parts are zero for lossless models.

the aspect ratio of the $\vec{B}$ ellipse and $|\vec{B}|_{\max}$ and $|\vec{B}|_{\min}$ the lengths of the principal axes of this ellipse.

C. Example: Exclusion of Losses

To illustrate the individual role of the dependencies in (17), the static nonlinear and anisotropic reluctivity model in [9] is considered here for extracting a time-harmonic anisotropy model that excludes losses. Since loss data are not available, the arguments α_{rd} and α_{td} of the complex-valued reluctivity tensor entries are set to zero. For a large set of parameters $\{|\vec{B}|_{\max}, a, \gamma\}$, the effective reluctivity tensor entries are computed as the average value of ν_{rd} and ν_{td} over one period of the $\vec{B}$-locus. Fig. 1 shows the entries of $\nu(|\vec{B}|_{\max}, a, \gamma)$ at $|\vec{B}|_{\max} = 0.55$ T, $|\vec{B}|_{\max} = 1.38$ T and $|\vec{B}|_{\max} = 1.93$ T. The scales are not equally set, to better observe some details. The following general conclusions can be drawn:

- If $|\vec{B}|_{\max}$ increases, the reluctivity tensor entries increase as well, since the material is operated closer to the saturation level.

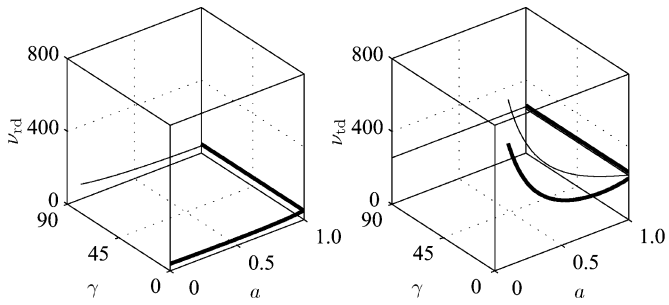

Fig. 2. Moduli $\nu_{\rm rd}$ and $\nu_{\rm td}$ [m/H] of the reluctivity tensor entries as a function of the aspect ratio a [−] and the inclination angle γ [°] of the $\vec{B}$-locus, for $|\vec{B}|_{\rm max} = 0.5$ T (thin solid line) and $|\vec{B}|_{\rm max} = 1.0$ T (thick solid line).

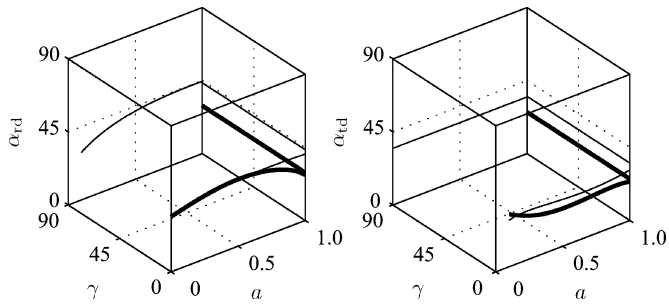

Fig. 3. Arguments $\alpha_{\rm rd}$ and $\alpha_{\rm td}$ [°] of the reluctivity tensor entries as a function of the aspect ratio a [−] and the inclination angle γ [°] of the $\vec{B}$-locus, for $|\vec{B}|_{\rm max} = 0.5$ T (thin solid line) and $|\vec{B}|_{\rm max} = 1.0$ T (thick solid line).

- If $a = 1$, the $\vec{B}$-locus is circular and ν is independent of γ.
- If γ is small, the longest axis of the ellipse is close to the rolling direction and $\nu_{\rm rd}$ decreases with decreasing a, since $|\vec{B}|_{\rm rms}$ decreases as well. However, if in addition $|\vec{B}|_{\rm max}$ is very small, it is expected that $\nu_{\rm rd}$ starts increasing again when a approaches zero, because the material is operated in the Rayleigh region there.
- If γ is close to 90°, the longest axis of the ellipse is close to the transverse direction and the same behavior as in the previous item is observed for $\nu_{\rm td}$.
- If γ is close to 90° and a is close to zero, the $\vec{B}$-locus is almost linearly shaped and parallel to the transverse direction. As a consequence, $\nu_{\rm rd}$ takes up a high value there. When a starts growing, $\nu_{\rm rd}$ initially decreases due to the increasing component of $\vec{B}$ in the rolling direction. When a approaches unity, $\nu_{\rm rd}$ may increase again, provided $|\vec{B}|_{\rm max}$ is high enough to attain the saturation level.
- If γ and a are close to zero, the same behavior as in the previous item is observed for $\nu_{\rm td}$.
- If a is small, the $\vec{B}$-locus is almost linearly shaped and $\nu_{\rm rd}$ generally increases with γ, while $\nu_{\rm td}$ generally decreases with γ.

Neglecting one of these dependencies may have a considerable influence on the accuracy of the solution, even for isotropic materials where $|\vec{B}|_{\rm max}$ and a are the only parameters.

D. Example: Inclusion of Losses

In [8], it is described how $\underline{\nu}_{\rm rd}^{\rm re}$, $\underline{\nu}_{\rm rd}^{\rm im}$, $\underline{\nu}_{\rm td}^{\rm re}$, and $\underline{\nu}_{\rm td}^{\rm im}$ can be determined from measurements in the rolling and transverse direction of grain-oriented silicon steels, by processing the measured signals in the frequency domain. The measurements have been performed at 50 Hz on a square grain-oriented silicon steel sheet M111-35N of 80 mm length and 0.35 mm thickness.

The data in Figs. 2 and 3, respectively, represent the modulus and the argument of the complex reluctivity tensor entries, as measured in [8]. Although they only partially describe the relation $\underline{\nu}(|\vec{B}|_{\rm max}, a, \gamma)$, it is observed that Fig. 2 exhibits a similar behavior as the one shown in Fig. 1. By comparing Figs. 2 and 3, it is concluded that $\alpha_{\rm rd}$ and $\alpha_{\rm td}$ are much less sensitive to a and γ than $\nu_{\rm rd}$ and $\nu_{\rm td}$.

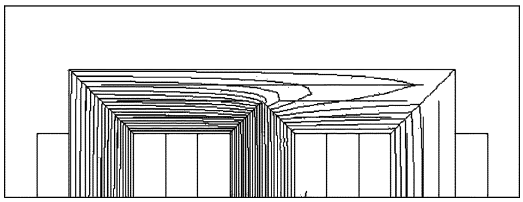

Fig. 4. Flux line distribution obtained with the time-harmonic real-valued anisotropy model in Fig. 1, if the initial phase angles of the currents in the coils are −85°, 35°, and 155°, respectively. The flux density in the middle limb is approximately 1.38 T.

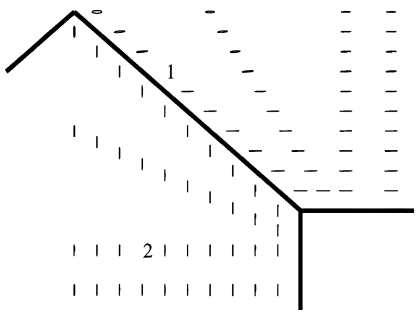

Fig. 5. Some flux density loci in the region close to the joint between the middle limb and the yoke of the transformer.

IV. Simulations

A. Example: Exclusion of Losses

The real-valued time-harmonic anisotropy model plotted in Fig. 1 is now used for simulating the no-load condition of a three-phase transformer. The flux line distribution, when the initial phase angles of the currents in the coils are −85°, 35°, and 155°, respectively, is plotted in Fig. 4. Fig. 5 shows some of the computed flux density loci in the region close to the joint between the middle limb and the yoke of the transformer. Rotational magnetization occurs close to the joints of the transformer, in contrast to the rest of the transformer where alternating magnetization prevails. The specific energy losses p [W/kg] [10] in each finite element

$$p = \frac{1}{\rho} \int_{t=0}^{T} \vec{H} \cdot \frac{\partial \vec{B}}{\partial t} \mathrm{d}t \tag{19}$$

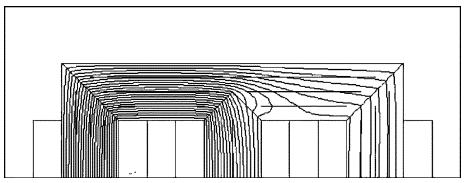

Fig. 6. Flux line distribution obtained with the time-harmonic complex-valued anisotropy model in Figs. 2 and 3, if the initial phase angles of the currents in the coils are $-85°$, $35°$, and $155°$, respectively. The flux density in the middle limb is approximately 1.17 T.

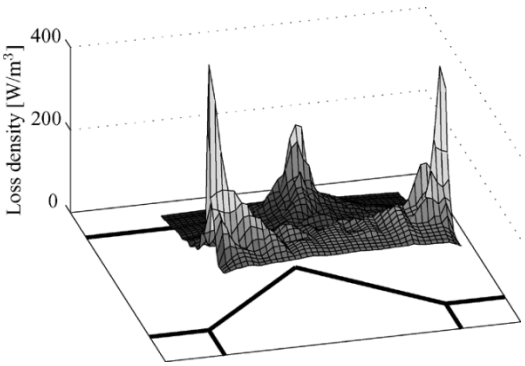

Fig. 7. Loss density distribution in the T-joint, obtained when simulating with the time-harmonic complex-valued anisotropy model.

where ρ is the specific mass of the material [kg/m^3], are zero here, but they can be estimated in a post-processing step by applying the obtained $\vec{B}$-loci to the input of some more advanced loss and/or hysteresis models.

B. Example: Inclusion of Losses

The three-phase transformer is now simulated using the complex-valued reluctivity tensor model in Figs. 2 and 3. Since these data are not related to those used in the previous analysis, the results cannot be compared. Fig. 6 shows the flux line distribution. It has to be assumed that all $\vec{B}$-loci are circular, i.e. $a = 1$ and γ irrelevant, for determining the value of the reluctivity tensor entries, since too limited data are available. More data are required to perform a more accurate simulation.

Here, the use of a complex reluctivity tensor allows to estimate the specific losses in each finite element, by computing (19). This is shown in Fig. 7 for the region around the T-joint. Three loss peaks are observed. The two largest peaks are due to the elevated flux densities in the corners of the T-joint. The smallest peak occurs on top of the limb, where the magnitude of the flux density is smaller. However, in this area, rotational fields are prevalent. Hence, this peak indicates the increased losses due to rotational magnetization.

V. Conclusion

Time-harmonic analyses are useful for simulating the steady state operation of a device. This is particularly attractive in the early design stages of new devices, since the main parameters can be extracted quickly. However, when compared to transient analysis, additional errors are introduced, since the time-variation of the reluctivity tensor over one period cannot be modeled as such. In this paper, the traditional concept of using effective reluctivity curves for time-harmonic analyses, is generalized. The generalization is based on the properties of the elliptic path the flux density vector describes in each finite element. The approach can be used for modeling nonlinear and anisotropic materials. Losses due to hysteresis or rotational fields can be implicitly included, by allowing the reluctivity tensor entries to have complex-valued entries. Two examples are presented in order to illustrate the anisotropic and lossy character of the solution. Additional research should be performed on the averaging rules and on the practical extraction of all the required data, in order to fully assess the capabilities of this technique.

Acknowledgment

The first author has been affiliated with Atlas Copco Airpower n.v. since May 1, 2005. The research was performed at the Katholieke Universiteit Leuven, ESAT-ELECTA, Kasteelpark Arenberg 10, B-3001, Heverlee, Belgium.

References

[1] K. J. Binns, P. J. Lawrenson, and C. W. Trowbridge, *The Analytical and Numerical Solution of Electric and Magnetic Fields*. Chichester, U.K.: Wiley, 1992.

[2] D. Lederer, H. Igarashi, and A. Kost, "The Newton-Raphson method for complex equation systems," *Appl. Comput. Electromagn. Soc. J.*, vol. 12, pp. 113–116, 1997.

[3] H. Vande Sande, F. Henrotte, and K. Hameyer, "The Newton-Raphson method for solving nonlinear and anisotropic time-harmonic problems," *Int. J. Computation and Mathematics in Electrical and Electronic Engineering (COMPEL)*, vol. 23, no. 4, pp. 950–958, 2004, to be published.

[4] J. Luomi, A. Niemenmaa, and A. Arkkio, "On the use of effective reluctivities in magnetic field analysis of induction motors fed from a sinusoidal voltage source," in *Proc. Int. Conf. Electrical Machines (ICEM 86)*, vol. 2, Munich, Germany, Sep. 1986, pp. 706–709.

[5] G. Paoli, O. Bíró, and G. Buchgraber, "Complex representation in nonlinear time harmonic eddy current problems," *IEEE Trans. Magn.*, vol. 34, no. 5, pp. 2625–2628, Sep. 1998.

[6] E. Vassent, G. Meunier, and J. C. Sabonnadière, "Simulation of induction machine operation using complex magnetodynamic finite elements," *IEEE Trans. Magn.*, vol. 25, no. 4, pp. 3064–3066, Jul. 1989.

[7] R. D. Findlay, N. Stranges, and D. K. MacKay, "Losses due to rotational flux in three phase induction motors," *IEEE Trans. Energy Conversion*, vol. 9, no. 3, pp. 543–549, Sep. 1994.

[8] M. Birkfeld, "Investigation of the permeability tensor of electrical steel sheet," *IEEE Trans. Magn.*, vol. 34, no. 5, pp. 3667–3673, Sep. 1998.

[9] H. Vande Sande, T. Boonen, I. Podoleanu, F. Henrotte, and K. Hameyer, "Simulation of a three-phase transformer using an improved anisotropy model," *IEEE Trans. Magn.*, vol. 40, no. 2, pp. 850–855, Mar. 2004.

[10] H. Pfützner, "Rotational magnetization and rotational losses of grain-oriented silicon steel sheets—Fundamental aspects and theory," *IEEE Trans. Magn.*, vol. 30, no. 5, pp. 2802–2807, Sep. 1994.

Manuscript received June 8, 2004.